Engineering Structures 294 (2023) 116801

Contents lists available at ScienceDirect

Engineering Structures

journal homepage: www.elsevier.com/locate/engstruct

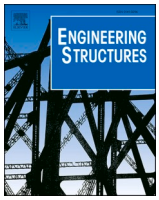

Damping in masonry arch railway bridges under service loads: An experimental and numerical investigation

Emrah Erduran [a,*], Semih Gonen [b], Bora Pulatsu [c], Serdar Soyoz [d]

[a] Department of Built Engineering, Oslo Metropolitan University, Oslo, Norway
[b] Department of Civil and Environmental Engineering, Universitat Politècnica de Catalunya, C/ Jordi Girona, 1-3, Barcelona 08034, Spain
[c] Department of Civil and Environmental Engineering, Carleton University, Ottawa, ON K1S 5B6, Canada
[d] Department of Civil Engineering, Bogazici University, Bebek, Istanbul, Turkiye

ARTICLE INFO

Keywords:
Damping ratio
Masonry arch bridge
In-service bridges
Train loading
Discrete element method
Discrete-continuum modeling

ABSTRACT

This article investigates the damping behavior of masonry arch bridges under service loads extracted from experimental data and provides guidelines on how to emulate this behavior in numerical analysis, particularly in discrete element model applications. First, an experimental campaign is undertaken and vibrations on three masonry arch railway bridges under train loads were monitored. The modal damping ratios from several sensors on each bridge were extracted by isolating the modal component of free decay vibrations which commence immediately after the train leaves the bridge. The modal damping ratios identified under service loads were compared with their counterparts identified under ambient vibrations. The suitability of mass-proportional, stiffness-proportional and Rayleigh damping models in emulating damping in masonry arch bridges was evaluated. In the numerical phase of the study, a single-arch masonry bridge was modeled using mixed discrete continuum approach and a moving load analysis was conducted without applying any additional viscous damping. The results of the numerical analysis indicate that the inherent damping in discrete element models provided by their nonlinear nature can be sufficient to emulate the damping behavior of masonry arch bridges under service loads. The research provided in this article is unique in the sense that it combines an experimental study and a numerical study on damping of masonry arch bridges under service loads. Unlike its counterparts in literature, which use either ambient vibrations or seismic action, damping values are computed under appropriate levels of vibration amplitudes for service loads, which is critical to estimate the modal damping ratios accurately under these loads.

1. Introduction

Masonry arch bridges are a significant feature of the European road and railway networks, with more than 40% of railway bridges and 25% of road bridges being of this type [1,2]. In Turkey, over 12% of the railway bridges and approximately 29% of the culverts are masonry arch structures. Additionally, there are over 2,000 masonry arch bridges in the Turkish road network. These bridges are not only important for the transportation network but also have cultural and architectural significance. However, their safety and continued use are threatened by factors such as material decay, fatigue, strength degradation, changes in boundary conditions, and increased traffic loads over time. As such, structural analysis of masonry arch bridges has received significant attention in the last decades [3]. Most of the studies focused on the numerical analysis of masonry bridges under vertical loading for service conditions [4–11], or under horizontal loading under seismic actions [12–18], or under support settlements caused by scour actions [19,20]. Researchers used different experimental approaches to calibrate their numerical models and to attain better approximations of the physical behavior [21–28]. Amongst these approaches, operational modal analysis (OMA) or modal identification using vibration signatures is the most common strategy as it allows obtaining the dynamic properties, such as modal frequencies, damping ratios, and mode shapes, pertaining to the global behavior of structures [29–38].

Of these parameters, damping remains arguably the most elusive because, unlike stiffness and mass, it cannot be defined directly from the geometric and material properties. Therefore, empirical data on damping provides valuable information for accurately modeling this

* Corresponding author.
E-mail address: emrahe@oslomet.no (E. Erduran).

https://doi.org/10.1016/j.engstruct.2023.116801
Received 18 April 2023; Received in revised form 9 July 2023; Accepted 21 August 2023
Available online 26 August 2023

parameter. In literature, several studies [29–38] estimated the modal damping ratios of masonry arch bridges under ambient vibrations when the bridge was closed to the traffic and reported that these values vary between 0.5 and 4%, where the first mode damping ratio rarely exceeded 2%.

However, damping of a structure is dependent on the type of excitation and its amplitude, and the damping ratio under higher vibration amplitudes can be much higher compared to those obtained from ambient vibrations. This observation is confirmed by a rare example of dynamic identification of a masonry arch bridge under service conditions [39], where the damping ratios under service loads were measured between 2 and 6%; significantly higher than those obtained under ambient vibrations. As the dynamic analysis of masonry arch bridges under service conditions requires accurate representation of the damping in the bridge, there is clearly a need for more empirical data on the modal damping ratios of masonry bridges under service loads.

In addition to the experimental studies that are mainly conducted under ambient vibrations, there are also several studies that focus on the response of masonry arch bridges to seismic actions. The damping aspect of the dynamic response of masonry arch bridges has also been studied extensively in these studies. Research that focus on railway bridges [9,24,40] and their dynamic behavior under seismic loads [41–44] are mainly numerical studies and their suggestions aim to ensure that the numerical analysis can be conducted in a reasonable time and does not lead to overdamping in the first mode [43,45,46]. As such most of the numerical studies, in particular those that use discreet element method, either ignore damping completely assuming that undamped models will provide conservative results or strive to emulate stiffness-proportional damping, which is assumed to be the most reliable option but comes at a very high computational cost in discrete element method applications. Mass-proportional part of Rayleigh damping is avoided as it is considered to provide unconservative estimates of the ultimate limit state of the arches [47–49]. Although, these arguments make valid points, none of them are based on physical data that has been experimentally confirmed either through field tests or laboratory experiments. In other words, there is a gap in the literature on how the energy is dissipated in masonry arch bridges, especially under service loads because most of the experimental studies use data from ambient vibrations while the numerical research focus on seismic analysis.

The current study addresses this gap by presenting an overview of modal damping ratios extracted from measurements on three masonry arch railway bridges under train loads. A locomotive was driven multiple times on each bridge at different speeds and both the forced vibrations created by the locomotive and the vibrations in the free decay phase which starts immediately after the locomotive leaves the bridge were recorded with several accelerometers. The vibrations during free decay after each train crossing are then decomposed into its modal components and the damping at each modal frequency was estimated at each sensor. Through analysis of the extracted damping values for several cases, the variation of damping in masonry arch bridges with modal frequency is established. Then, we conducted a numerical analysis where we analyzed the dynamic response of a single-span masonry arch bridge under moving loads. A mixed discrete-continuum approach, presented previously in other studies [7,50–52], is utilized to perform moving load analysis without considering damping to evaluate if the energy dissipation through inherent inelastic action in this modeling approach is enough to justify not using damping in such models under service loads.

The research presented in this article stands out due to its distinct approach of integrating both experimental and numerical investigations to examine the damping characteristics of masonry arch bridges when subjected to service loads. In contrast to existing studies that primarily focus on ambient vibrations or seismic actions, this research specifically estimates damping values using vibration amplitudes that are relevant to service loads. As a result, this study provides valuable insights that go beyond existing literature, contributing to a better understanding of damping behaviour in masonry arch bridges under service loads, which is essential for reliably estimating the vibration levels on bridges under service loads both for ballast stability and passenger comfort [53]. Further, the study uses moving load analysis on a mixed discrete-continuum model including all parts of the bridge such as spandrel walls which has been rarely addressed in the literature. Combining a mixed discrete-continuum model with a moving load analysis, we could capture the response of the masonry arch bridge under dynamic loads including the potential nonlinear behavior of the bridge through different mechanisms such as inter-block joint openings, sliding, friction between different parts, and plastic deformation within the continuous medium. This modeling approach allowed us to capture the energy dissipation inherent in the mixed discrete-continuum model and accurately evaluate the need for additional viscous damping in such models under service loads.

2. Experimental campaign

Vibrations on three different masonry arch bridges were measured during and after train crossing. All three bridges are located on the same railway along with several other masonry arch bridges [33]. These bridges represent similar designs: number of spans, barrel arches, sandstone or limestone, mortar and infill as a building material, and a similar deck width of around five meters. Geometric properties of the bridges are presented in Table 1. Bridges 13, 41 and 5 have three, four and five arches, respectively, as seen in Fig. 1-Fig. 3. These bridges were selected as they typify the groups of three-, four- and five-span bridges, and produced particularly clear results during the measurement campaign. Further details of the experimental campaign are presented in [30,33,54].

A cabled data acquisition system, force-balance accelerometers (FBA), and 24-bit recorders were used as instrumentation. Bridge 13 was equipped with 12 uniaxial FBA sensors during the vibration survey, while Bridges 41 and 5 had a setup of 20 FBA sensors. The sensors were placed longitudinally, vertically, and out-of-plane (transversely) over the arches and piers at the lateral edges of the deck to capture accelerations in three orthogonal directions as well as torsional rotations. Figs. 1-3 provide the sensor layout for the bridges. The system's sampling frequency was set to 200 Hz.

First, for each bridge, ambient vibrations were recorded continuously for approximately an hour. The ambient data was used to extract the natural modal frequencies, modal damping ratios, and the mode shapes of each bridge. Frequency Domain Decomposition (FDD) [55] technique is used for identifying the modal properties of a system based on its output response. Details of the system identification of the three bridges using different methods is previously summarized in [30]. Table 2 presents the frequencies of the first four modes of each bridge identified using the ambient vibrations when the bridges were closed to traffic. Also presented in Table 2 are the modal damping ratios estimated from the ambient vibrations. Considering the uncertainties in estimating the modal damping ratios under ambient vibrations, they are presented as a range rather than a single value.

On each bridge, a locomotive was driven six times with speeds between 20 km/h and 60 km/h and both the forced vibrations during the train crossing and the free decay after the locomotive leaves the bridge are recorded at each accelerometer. The locomotive, which is shown in Fig. 2, is a LDH125 type locomotive with four axles and a total weight of 70 tons. Its total length is 13.7 m with 2.5 m axle spacing. The

Table 1
List of presented bridges in this paper.

Bridge ID	Spans (m)	Total Length (m)	Max Height (m)
5	6-10-10-6-6	64.3	17.55
13	8-8-8	40.7	13.70
41	10-10-10-10	59.3	10.77

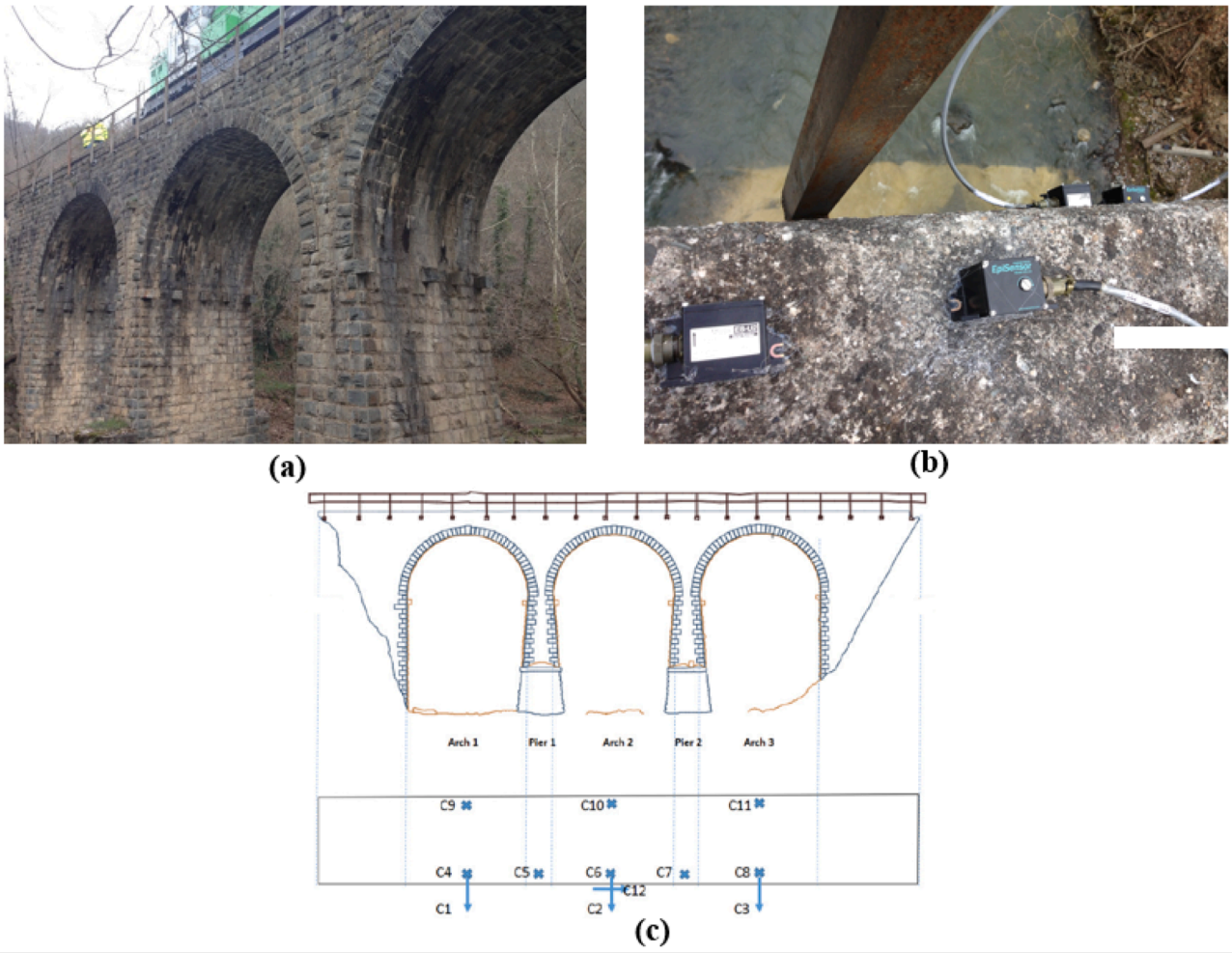

Fig. 1. (a) Bridge 13, (b) data collection, (c) sensor layout.

Table 2
Modal frequencies of the bridges identified from ambient vibrations.

	Bridge 5		Bridge 13		Bridge 41	
Mode Shape	f(Hz)	Modal Damping (%)	f(Hz)	Modal Damping (%)	f(Hz)	Modal Damping (%)
1st – transverse	6.01	0.43–1.32	6.23	0.45–1.00	5.72	1.22–4.44
2nd - transverse	8.50	0.06–0.33	8.37	0.97–1.30	8.49	1.02–1.56
3rd - transverse	10.55	0.27–0.44	9.98	0.79–1.14	15.33	1.16–3.57
1st - vertical	18.90	0.60–1.29	16.66	1.65–5.22	18.44	0.03–0.67

locomotive crossing created forced vibrations in both transverse and vertical directions. On average, 60 s long data was obtained during each locomotive crossing. Fig. 4 shows the train crossing data for Bridge 41 measured at sensor 12. It is easily noticed that the vibration amplitudes during train crossings are much higher than the ambient vibrations without traffic. Therefore, the damping under the train loads can differ significantly from those obtained under ambient vibrations.

3. Damping in structures: a brief overview

In the dynamic response analysis of multi-degree-of-freedom systems, obtaining the damping matrix arguably provides the biggest challenge because, unlike the mass and the stiffness matrices, it cannot be directly determined from the structural dimensions and material properties. Therefore, it is common to specify the damping in structures via numerical values for the modal damping ratios. These modal damping ratios can then be combined to construct the damping matrix of the structure.

The modal damping ratios of structures are estimated from the vibrations recorded on the structures. However, it is impractical to measure the vibrations in each structure. Further, it is clearly impossible to measure the damping properties of a structure that will be designed and is yet to be constructed. Thus, we rely on empirical data that has been previously gathered from similar structures. However, damping in structures depends also on the amplitude of the vibrations and, thus, not all data gathered on similar structures is necessarily fit for use if the vibration amplitudes during the vibration measurements are very different from the vibration amplitudes expected under the analysis loads. For example, Chopra [56] summarizes that the modal damping ratios in the Millikan library building varies from approximately 1% under low-amplitude forced vibration tests to 3% when the building is subjected to relatively small earthquake motion to 7% under a strong

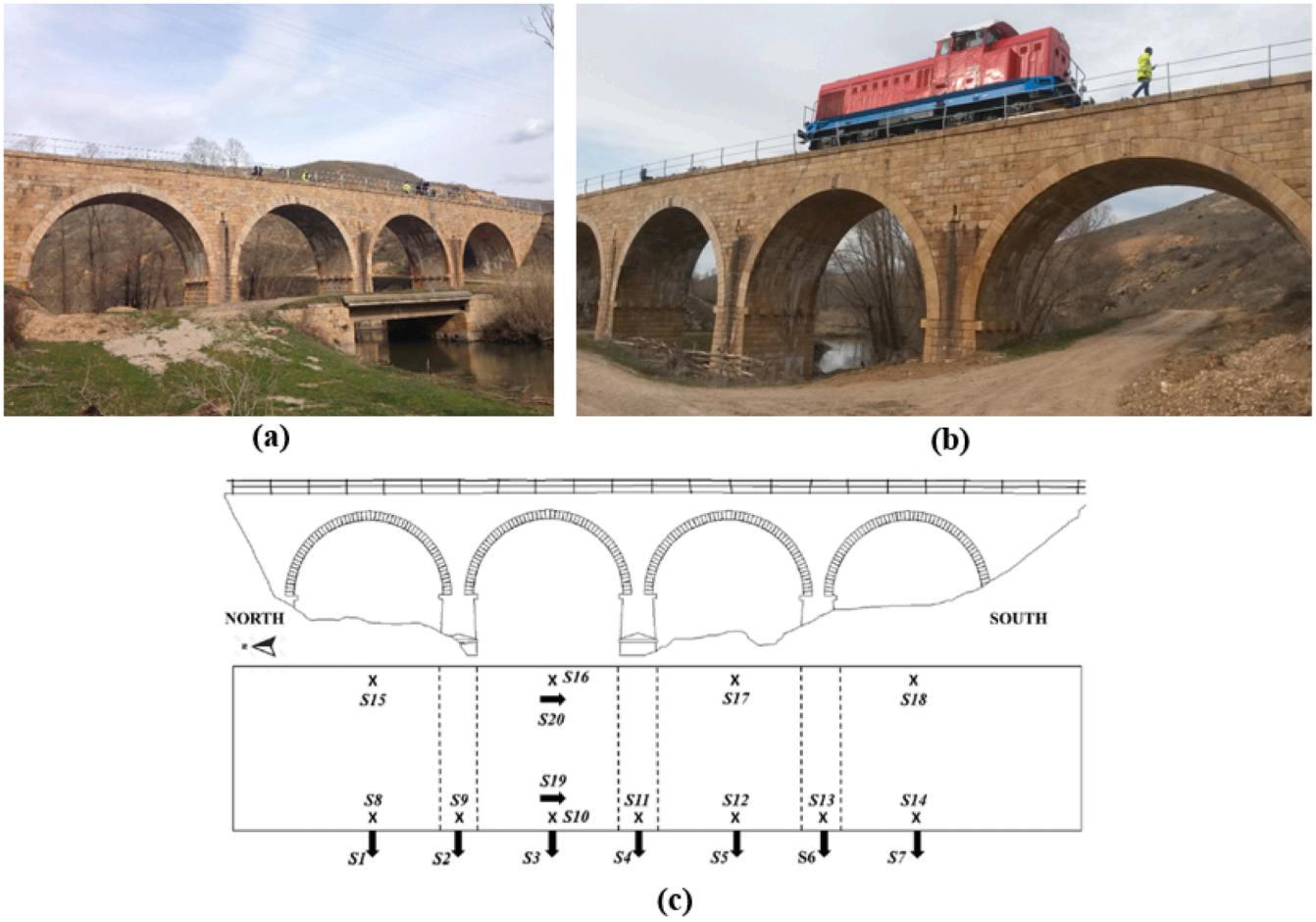

Fig. 2. (a) Bridge 41, (b) train crossing, (c) sensor layout [54].

earthquake motion. Thus, the modal damping ratios that will be used in the numerical analysis should be chosen carefully from data for similar structures under similar vibration amplitudes. Similarly, modal damping ratios extracted from ambient vibration tests may vary significantly from those under service loads and, thus can be unfit to use in numerical analysis under such loads.

Once the modal damping ratios are specified, they can be combined to create the damping matrix using different approaches. Rayleigh damping and its two variations, mass-proportional damping and stiffness-proportional damping, are arguably the most widely used classical damping models. In mass-proportional and stiffness-proportional damping, the damping matrix is related to mass and stiffness matrices through $\mathbf{C} = a_o\ \mathbf{M}$ and $\mathbf{C} = a_1\ \mathbf{K}$, respectively. The coefficients a_o and a_1 can be computed as $a_0 = 2\xi_i\omega_i$ and $a_1 = 2\xi_i/\omega_i$ where ω_i and ξ_i are the frequency and the damping ratio of the i^{th} mode at which the models are anchored. Used alone, the two models provide very different damping-frequency curves as shown in Fig. 5. One of the main shortcomings of these two models is that they can only control the modal damping ratio at one modal frequency.

Rayleigh damping overcomes this shortcoming by combining these two models into a single model and defines the damping matrix as: $\mathbf{C} = a_o\ \mathbf{M} + a_1\ \mathbf{K}$. The coefficients a_o and a_1 can be determined from the specified modal damping ratios ξ_i and ξ_j at the respective modal frequencies ω_i and ω_j by solving the linear system of equations:

$$\frac{1}{2}\begin{bmatrix} 1/\omega_i & \omega_i \\ 1/\omega_j & \omega_j \end{bmatrix}\begin{Bmatrix} a_0 \\ a_1 \end{Bmatrix} = \begin{Bmatrix} \xi_i \\ \xi_j \end{Bmatrix} \tag{2}$$

The damping ratio of the n^{th} mode can then be computed as:

$$\xi_n = \frac{a_0}{2}\frac{1}{\omega_n} + \frac{a_1}{2}\omega_n \tag{3}$$

The resulting damping-frequency curve is plotted in Fig. 5. By prescribing the modal damping ratio at two modal frequencies, Rayleigh damping provides an improved control of the damping behavior of the structure compared to mass- and stiffness-proportional damping models and used often in dynamic analysis of structures.

4. Extraction of damping ratios from experimental data

To evaluate the damping of masonry arch bridges under service loads, we extracted the modal damping ratios from the vibrations in the free-decay stage after each train crossing. The steps of this extraction process, which has been repeated for each bridge, each train crossing, and each natural frequency given in Table 2 are summarized below:

1. For each sensor, visually identify the two points in time when the free-decay phase of the vibration starts and ends. These two points form the basis for modal damping extraction using the principle of decay of motion [56].

2. For each modal frequency, extract the narrowband component of the free decay vibration. In this study, we used band-pass filtering for this purpose. The width of the band-pass filter was set to 0.2 Hz to avoid any interference from other frequencies that can be associated with the train-track system (loading) or other modes of the bridge.

3. The narrowband free-decay vibration for each modal frequency represents the free-decay vibration of the equivalent single-degree-of-freedom system. The envelope curve of the narrowband free-decay vi-

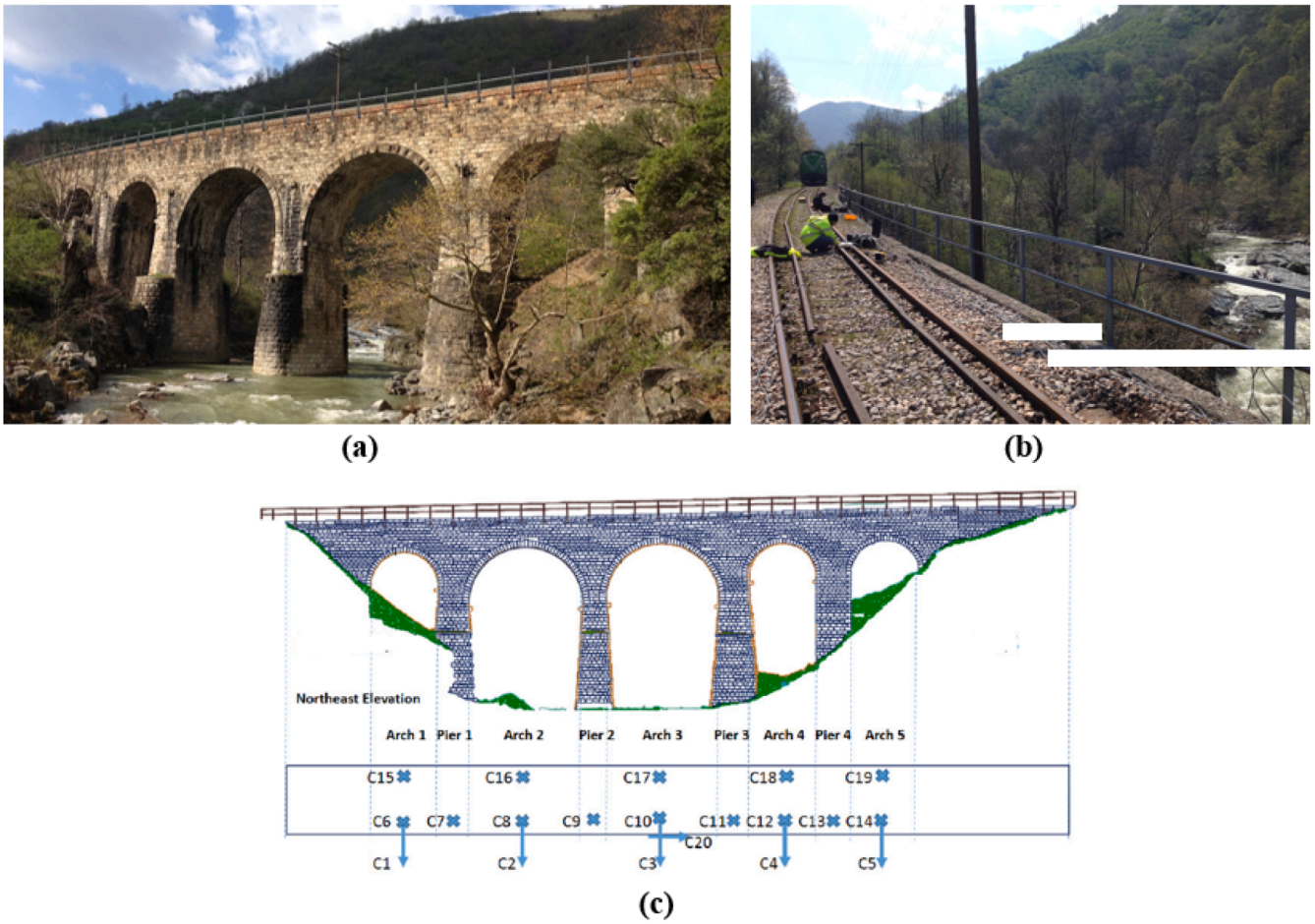

Fig. 3. (a) Bridge 5, (b) test preparation, (c) sensor layout.

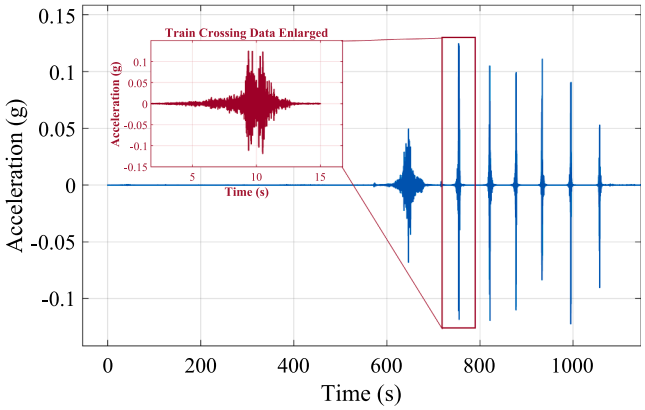

Fig. 4. Data of the train crossings over Bridge 41 recorded by sensor 12.

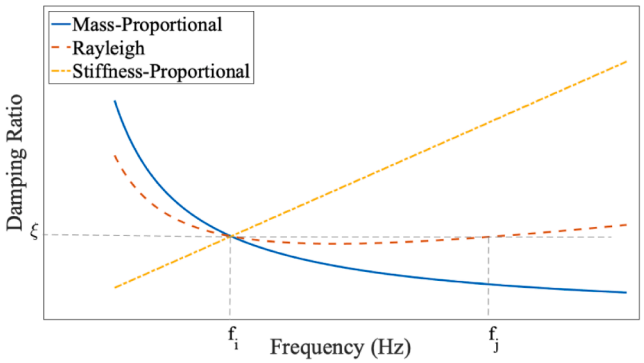

Fig. 5. Variation of damping ratio with frequency for different damping models.

brations can be represented by the equation $\mp\rho e^{-\xi_n w_n t}$ where

$$\rho = \sqrt{[u(0)]^2 + \left[\frac{\dot{u}(0) + \xi_n \omega_n u(0)}{\omega_D}\right]^2} \tag{4}$$

In Eqn.4, $u(0)$ and $\dot{u}(0)$ are the initial displacement and velocity of the free-decay motion, respectively, ξ_n is the modal damping ratio, and ω_n and ω_D are the undamped and damped natural frequencies, respectively.

4. Fitting an exponential function, $f(t) = ae^{bt}$ where a and b are the equation constants to the narrowband free-decay motion, the modal damping ratio for each modal frequency can be computed from $b = -\xi_n \omega_n$ since ξ_n is the only unknown in this expression.

An example application of this procedure is summarized next. Fig. 6 (a) depicts the vibrations recorded in the transverse direction at the middle of the second arch of the four-span bridge, i.e. sensor number 3 shown in Fig. 2(c), during the crossing of the train. In this figure, the free-decay part can be identified between approximately t = 10.5 s and t = 14.0 s; see Fig. 6(a). For the first modal damping ratio, a bandpass filter with a window of 5.6 Hz to 5.8 Hz is applied to the free-decay motion and the resulting narrowband component is plotted in Fig. 6 (b). Also plotted in Fig. 6(b) is the exponential curve fitted to the

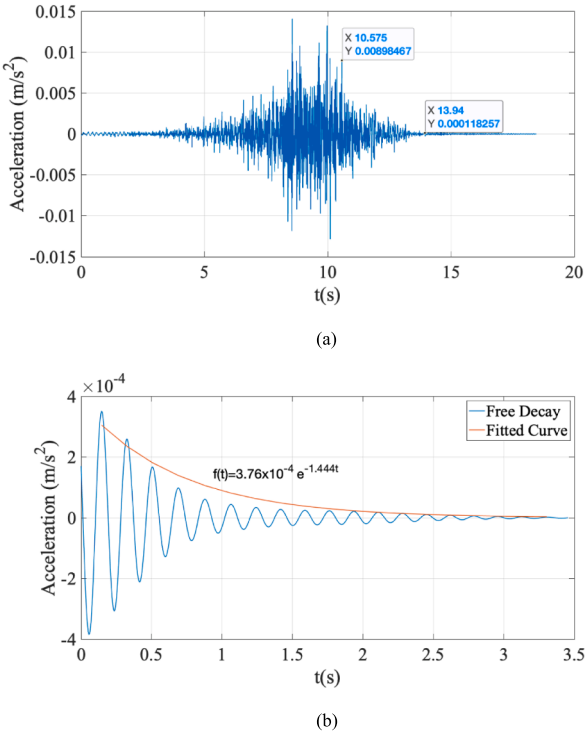

Fig. 6. (a) Vibration data recorded at the middle of the second arch on the four-span bridge (sensor 3 in Fig. 2(c)) during a train crossing (b) narrowband free-decay data for the first natural frequency and the fitted curve.

narrowband component together with its equation. Using the relationship $b = -\xi_1\omega_1$ and setting $b = -1.444$ and $\omega_1 = 5.72Hz*2\pi$ rad/s, the modal damping ratio for this case can be computed as, $\xi_1 = 4.02\%$. The same procedure was repeated for each of the four modal frequencies given in Table 2.

This procedure is repeated for the vibrations recorded at each sensor and each train crossing for each of the four modes. For the transverse modes, vibration data from the sensors located along the transverse direction in the middle of each arch (for example, sensors 1, 3, 5, and 7 in Fig. 2(c)) is used while data from the vertical sensors (sensors 8, 10, 12, and 14 in Fig. 2(c)) is used for the vertical mode. As a result, for each mode, 24 modal damping ratios from four sensors and six train crossings were extracted for the four-span bridge. Each of the extracted modal damping ratios is depicted with a blue marker in Fig. 7. Also shown in Fig. 7 are the mean values for the model damping ratio at each natural frequency represented by an orange circle along with a trendline (power function) that is fitted to the data. It is clear from Fig. 7 that the damping is higher for lower frequencies for the four arch masonry arch bridge under service loads and decreases consistently as the frequency increases.

To be able to evaluate the variation of modal damping ratio with the geometry and the vibration frequency of masonry arch bridges under service loads, we repeated the procedure summarized above for the three- and five-arch bridges. For each bridge, the train crossed the bridge six times and the data was collected in transverse and vertical directions at the middle of each arch. As a result, 18 modal damping ratios was obtained for each modal frequency for the three-arch bridge while 30 modal damping ratios was extracted for the five-arch bridge. Fig. 8 shows the modal damping ratios for each bridge for four modal frequencies along with a fitted trendline which is presented solely to better visualize the trend of the data. Although the steepness of the curve, which indicates the rate of decline in the modal damping ratio with the modal frequency changes from one bridge to the other, the general trend is the same for each bridge: The modes with lower frequencies have higher modal damping ratios and the modal damping ratio decreases with an increase in the modal frequency for masonry arch bridges under service loads. Considering that, in stiffness-proportional damping models, the modal damping ratio increases with modal frequency, which contradicts with the empirical data presented herein, we can confidently state that stiffness-proportional damping model is not suitable for dynamic analysis of masonry arch bridges under service loads.

Further, the damping ratios identified under service loads are consistently higher than those identified from ambient vibrations because of the higher vibration amplitudes under the service loads. This observation confirms that the empirical modal damping ratios obtained from ambient vibrations may not be fit for use in dynamic analysis of masonry arch bridges under service loads.

As the next step, we evaluated the possibility of using mass-proportional and Rayleigh damping models anchored at different frequencies to emulate the damping in masonry arch bridges. For this, for each bridge, we used four different alternatives that defines the relationship between the modal damping ratio and the modal frequencies: mass-proportional damping anchored at the first modal frequency and Rayleigh damping anchored at three different modal frequency pairs: first and second, first and third, and first and fourth. In this article, we used the mean modal damping ratio computed from the extracted damping values for each modal frequency, which are represented by orange dots in Fig. 9, to define the mass-proportional and Rayleigh damping curves for each bridge. As such, all the curves given in Fig. 9 intersect the mean modal damping ratio at the respective first modal frequency. Further, Rayleigh damping models anchored at the second, third, and fourth modal frequencies intersect the mean modal ratios at the respective frequencies.

The efficacy of different damping models to emulate the modal damping ratios extracted from experimental campaign somewhat vary

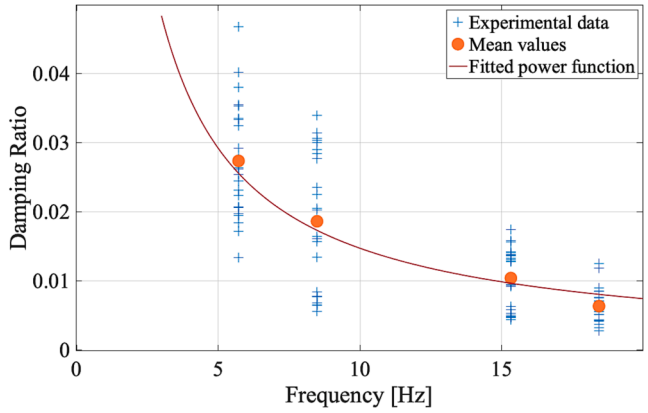

Fig. 7. Modal damping ratios for the four-arch bridge (Bridge 41).

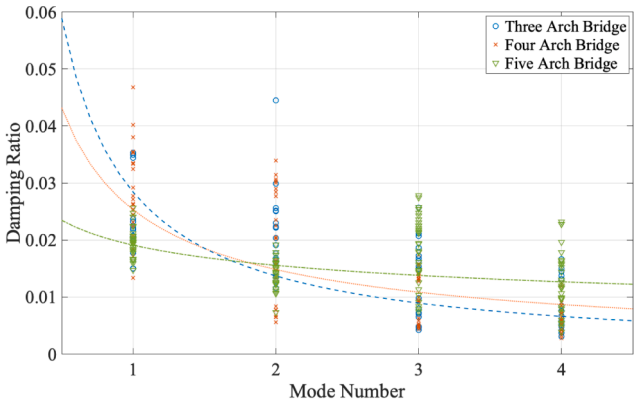

Fig. 8. Variation of modal damping ratio with frequency.

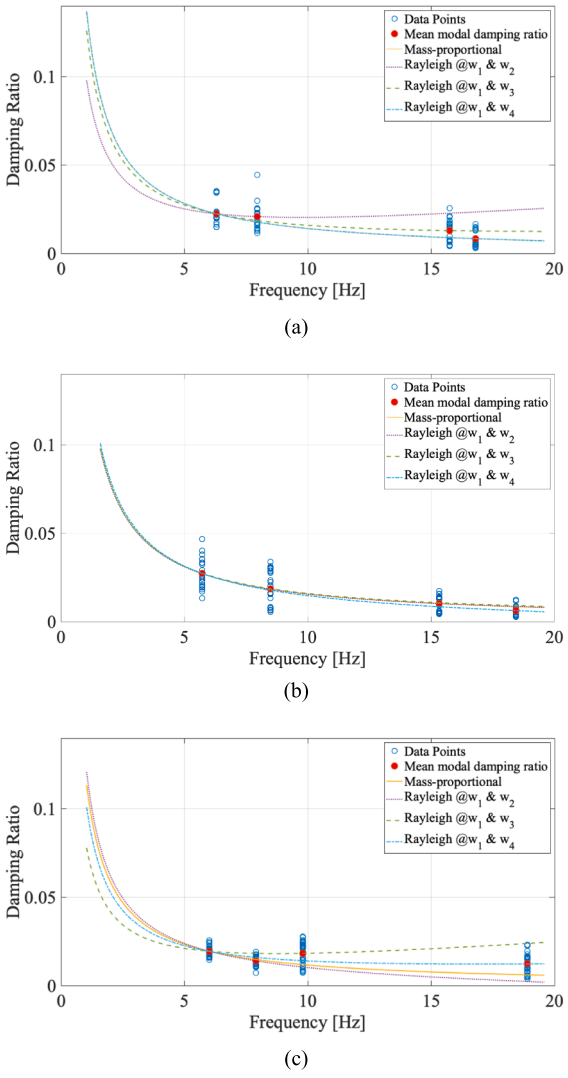

Fig. 9. Damping models for (a) three-arch (b) four-arch and (c) five-arch masonry arch bridges under service loads.

from one bridge to the other. For the three-arch bridge (Fig. 9 (a)), Rayleigh damping model anchored at the first and second frequencies overestimates the modal damping ratios at the third and fourth modal frequencies significantly. Similarly, the Rayleigh damping curve anchored at the first and third modal frequencies of the five-span bridge (Fig. 9 (c)) has increasing damping ratios for frequencies higher than the third mode frequency and, thus, overestimates the modal damping ratio at the fourth modal frequency. These two cases show that, anchoring the Rayleigh damping at the second or third frequency can lead to increasing modal damping ratios for higher frequencies, which is not consistent with the experimental data. On the other hand, Rayleigh damping anchored at the first and fourth modal frequencies emulates the modal damping ratios for each of the bridges in a satisfactory manner. This observation is not surprising given the fourth mode is the highest mode considered in this study and anchoring the Rayleigh damping at this modal frequency in addition to the first modal frequency defines the boundaries for the modal damping ratios for each of the modes considered. To generalize this observation, we can rephrase the previous sentences as: Rayleigh damping model anchored at the first and n^{th} modal frequencies, n being the highest mode number considered in the analysis, provides very good estimates of the modal damping ratios for all the modes considered. In contrast, Rayleigh damping anchored at the first and i^{th} modal frequencies ($i < n$) can lead to unreasonably higher modal damping ratios for the frequencies higher than the i^{th} modal frequency.

An interesting observation from Fig. 9 is the accuracy of the mass-proportional damping model in estimating the modal damping ratios for all three bridges. Because it is anchored at only one modal frequency, which is generally the first mode, mass-proportional damping does not provide the same level of control to the analyst as Rayleigh damping. Despite this limitation, the damping ratio – frequency curves provided by the mass-proportional damping model follow the experimental modal damping ratios very closely for all three bridges. Further, for the three-span and four-span bridges, mass-proportional damping and Rayleigh damping anchored at the first and fourth modal frequencies are virtually identical to each other.

One of the main shortcomings of the mass-proportional damping has been reported to be the very high modal damping ratios assigned to the frequencies lower than the first mode frequency [47–49]. The modal damping ratios at the frequencies lower than the first modal frequency become significant when the frequency of the bridge is reduced by the damage sustained by the structure under extreme events. While this is a legitimate concern for seismic analysis where the bridge is likely to sustain high levels of damage in a relatively short time, there is no danger for such high levels of damage that will lead to drastic changes in the first modal frequency under service loads. As such, use of mass-proportional damping provides a very attractive alternative to Rayleigh damping for dynamic analysis of masonry arch bridges under service loads particularly if explicit numerical integration algorithms are used in the analysis because of the computational cost of the stiffness-proportional component of the Rayleigh damping. Specifically, the critical time step, i.e., $\Delta t < 2/\omega_{max}\left(\sqrt{1+\xi_{max}^2}-\xi_{max}\right)$, required to ensure numerical stability during explicit numerical solutions, reduces drastically when stiffness proportional component of the Rayleigh damping model is used compared to the case when only the mass proportional component is used(i.e., $\Delta t < 2/\omega_{max}$) [47].

So far, we anchored the damping models at the modal damping ratios extracted from the experiments. However, rarely an analyst has experimental data to use for the modal damping ratios and relies on the values provided in literature. As such, it is important to suggest values for the modal damping ratios at the modal frequencies to provide an analyst with all the tools needed to conduct a dynamic analysis. Since we suggest use of only the first and fourth modal frequencies in defining the damping models, we will focus on the modal damping ratios at these two frequencies. Further, the values of the modal frequencies for the first and fourth modes for the three bridges are very close to each other (Table 2) allowing us to combine all the data for the three bridges at these frequencies. Due to the limited amount of data used, we decided to refrain from directly using detailed statistical analysis of the extracted modal damping ratios at these modal frequencies for the suggestions. Instead, taking a close look at the extracted modal damping ratios for the first and fourth modal frequencies for all three bridges presented in Fig. 8 and the respective mean values, we propose to use 2.5% and 1.25% modal damping ratios at the first and fourth modal frequencies, respectively, in case the analyst chooses to use the Rayleigh damping. For the mass-proportional damping use of 2.5% damping at the first modal frequency would suffice.

We would like to emphasize the fact that modal properties of masonry arch bridges may significantly change for different bridges. However, for the similar typology of bridges used in this study, the first few mode shapes generally happen to be in the horizontal direction (either transverse or longitudinal) whereas the vertical modes are associated with higher modal frequencies that are difficult to obtain during the experiments or not in the range of interest for the analyst. Therefore, further experimental research should comprise a more general spectrum of bridges and allow refinement of the proposed values in this study.

5. Damping in discrete-continuum models of masonry arch bridges under service loads

In addition to viscous damping, which is the sole energy dissipation mechanism under service loads in macro models, in the adopted modeling strategy, the structure can also dissipate the energy exerted by the external loads via non-linear action at the joints as well as within the continuum. To investigate the inherent damping in the mixed discrete-continuum models under service loads, moving load analysis of a single-arch bridge was conducted without assigning any additional viscous damping to the bridge. In this section, first, a brief summary of mixed continuum-discrete approach and the numerical model developed will be provided and then the results of the numerical study will be explored.

5.1. Dynamic analysis via discrete-continuum-approach

Masonry arch bridges are composed of several load-bearing elements (e.g., soil backfill, arch barrel and piers), and they all interact under the external quasi-static and/or dynamic forces. To accurately predict the structural behavior of a masonry arch bridge, stone (or brickwork) skeleton and the soil backfill should be implemented in the computational model. In this study, the analyzed masonry bridge is modeled using a system of rigid and deformable blocks based on the discrete element method (DEM), denoted as the mixed discrete-continuum (MDC) approach. More specifically, the soil backfill is modeled as a continuous medium with an elasto-plastic material model, while the stone skeleton, which includes both the arch and the spandrel walls, is simulated using rigid blocks with six degrees of freedom (three translations and three rotations), as shown in Fig. 10. It is worth noting that the adopted computational modeling strategy addresses the mechanical interaction between the masonry units and the soil-masonry (or soil structure) within the discontinuum analysis framework. The proposed MDC model comprises of 1000 rigid blocks (Fig. 10(a)) and approximately 55,000 10-node high-order tetrahedra (Fig. 10(b)) elements that simulate the soil backfill behavior.

The mechanical interaction between the continuous medium and rigid blocks is simulated using normal and shear springs defined in orthogonal directions based on the point contact hypothesis [57,58]. Overlapping between the adjacent blocks is allowed, which is controlled by the defined normal (k_n) and shear (k_s) contact stiffnesses, as depicted in Fig. 11(a). At each point contact, the Coulomb-Slip joint model with tension cut-off is used, which uses tensile strength (f_T), cohesion (c) and joint friction angle (ϕ) (Fig. 11(a)) as the modeling parameters. Throughout this study, a brittle failure criterion is followed, which means that upon reaching the tensile strength, the tension capacity at the contact is set to zero. On the other hand, for the shear behavior, a residual frictional resistance is considered after passing the elastic limit in relative shear displacement. As shown in Fig. 11(b), the same contact

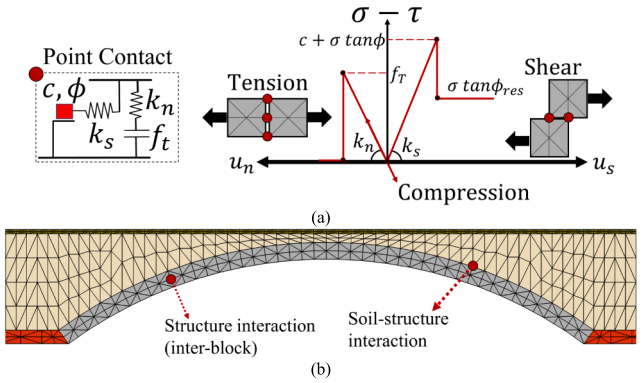

Fig. 11. (a) Point contact (illustrated in two dimensions) and adopted contact constitutive laws in normal and shear directions; (b) Representation of the inter-block and continuum discrete rigid block interaction.

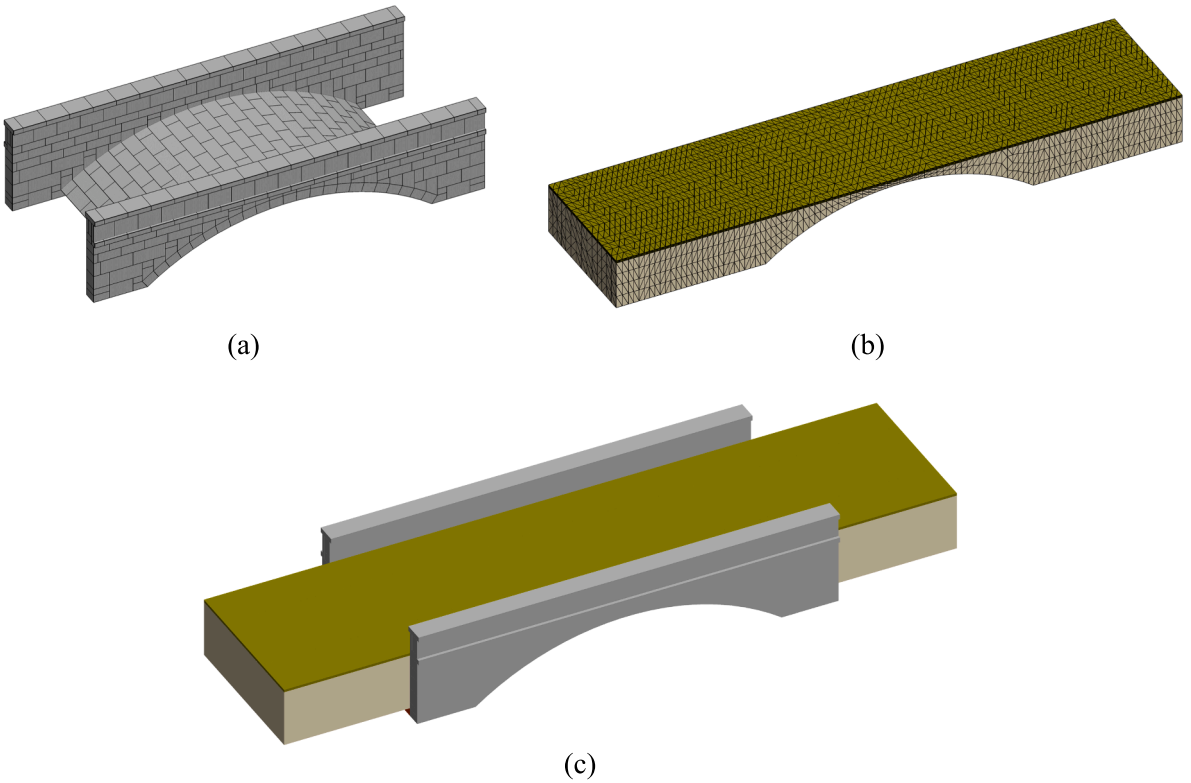

Fig. 10. Adopted computation model: (a) Stone skeleton (arch and spandrel wall) consisting of rigid blocks; (b) Continuum soil backfill; (c) Overall bridge configuration.

model is used for both masonry block interaction and soil-structure interaction, considering different mechanical properties. In the presented discontinuum model, the normal (σ_n) and shear ($\tau_{s,i}$) contact stresses are calculated as elastic increments ($\Delta\sigma_n$, $\Delta\tau_{s,i}$) based on the relative normal and shear point contact displacements (Δu_n, $\Delta u_{s,i}$). The computed elastic stress increments are added to the total contact stresses, computed in the previous time step, and updated (if applicable) following the determined failure criteria. Once the new contact stresses are obtained, they are multiplied with the associated contact area to get contact forces later used in the equations of motion as explained next.

The computational procedure of DEM relies on the explicit time marching scheme to predict gridpoint (or node) and rigid block velocities by solving the equations of motion using the central difference method. Note that the continuum is discretized into higher-order tetrahedral elements, and gridpoint movements are computed by integrating the equations of motion for each node. Unlike the continuous medium, for masonry blocks, new translational and rotational velocities are obtained at the mass center of each rigid block. Accordingly, the new velocities are utilized to update the position of the rigid block and gridpoints, which is further used to calculate relative contact displacements. The Mohr-Coulomb yield criterion is used as the plastic material model for the soil backfill. Briefly, at each time step, elastic (also called a trial) stresses are computed and added to the old ones. If the material becomes plastic, the new stress state is calculated by mapping the stress state back to the yield surface. Finally, the mixed discrete-continuum models are executed using a commercial three-dimensional discrete element code, 3DEC, developed by Itasca [59].

The analyzed masonry arch bridge has a 12-meter clear span, 1/6 rise to span ratio, 7.4 m width, 0.6 m spandrel wall thickness and 0.4 m arch thickness. The soil height above the keystone is 0.3 m, and the arch thickness does not change through the bridge span. The mechanical properties used in the MDC model are taken from the relevant literature studies (e.g., [6,7]) and are presented in Table 3.

5.2. Numerical analysis results

In the adopted modeling strategy used for simulating dynamic behavior of masonry arch bridges, energy dissipation takes place through the nonlinear actions at the joints as well as within the continuum. As such, the numerical model used in this study has two potential energy dissipating mechanisms: The first is the aforementioned nonlinear behavior while the second is the additional viscous damping that can be defined as Rayleigh damping or one of its components. Several studies propose ignoring additional viscous damping considering that the nonlinear nature of DEM provides sufficient energy dissipation [43,60,61]. However, most of these studies focus on seismic analysis where significant energy dissipation through nonlinear action is expected to occur and it is not certain that such a strategy would provide sufficient energy dissipation under service loads, which cause much lower vibration amplitudes in the bridge compared to seismic actions. These studies also do not address the MDC models.

To investigate the inherent damping in MDC models under service loads, we conducted a moving load analysis without assigning any additional viscous damping to the bridge. A moving load, representing a vehicle with a mass of 20 tons, was driven numerically over the bridge with a speed of 20 km/h. We monitored the vibrations at three points on the arch: Quarter point of the arch, middle of the arch, and top of the spandrel wall at the middle of the arch; points 1, 2, and 3, respectively in Fig. 12. Fig. 13 shows the time variation of the displacement at these three points under the effect of the moving load.

Analysis of the frequency content of the motion at these three points revealed that the motion at the quarter span (point 1 in Fig. 12) has the richest frequency content because, in a numerical analysis, the modes that are symmetrical about the mid-span are usually suppressed in the motions recorded at the mid-span and, are not visible in the frequency spectrum. Therefore, we decided to use the motion at point 1 to compute the modal damping ratios that are inherent in the MDC model. Fig. 14 depicts the power spectral density (PSD) of the vertical displacements recorded at the quarter span. Four frequencies clearly dominate the vertical motion at the quarter-span of the bridge as evidenced by the PSD.

We then applied the process detailed in section 3 to extract the modal damping ratios of the MDC model at these four modal frequencies. Fig. 15 shows the first and third modal componentś free decay of the vibrations recorded at the quarter point and the exponential curves fitted to these components to estimate the modal damping ratios. As a result of this process, we estimated the modal damping ratios as 3.22%, 1.69%, 1.49%, and 1.15% for the first four modal frequencies of the bridge. It should be reemphasized here that, these modal damping ratios represent the energy dissipation inherent in the MDC model through the nonlinear mechanisms in the joints such as inter-block joint openings, sliding, and plastic deformation within the continuous medium and no additional viscous damping was applied to the model.

Fig. 16 shows the modal damping ratios for the first four modes of the numerical model along with their counterparts extracted from the experiments. In this figure, we presented all the experimental results together without distinguishing between the different bridges because the modal damping ratios are presented for each mode number and not for the frequencies of the individual bridges. The data depicted in Fig. 16 clearly show that the inherent damping in the MDC model due to the nonlinear behavior in the joints is sufficient and no additional damping is required because the modal damping ratios of the numerical model are well within the experimental observations. Further, the numerical and experimental modal damping ratios follow the same pattern when it comes to their variation with the modal frequency.

However, it should be noted that the inherent damping in the MDC models depends very much on the modeling parameters used in the joints and can vary from model to model. As such, we propose a three-step process to ensure that the damping in the MDC models emulates the damping behavior of masonry under bridges under service loads.

i. Develop the MDC model and run an undamped moving load analysis.

Table 3
Material and contact properties used in mixed discrete-continuum model.

Material Properties - soil backfill				
Elastic Modulus (MPa)	Poisson's ratio (-)	Tensile strength (kPa)	Cohesion (kPa)	Friction angle (°)
150	0.2	5	50	60
Contact properties within the masonry block				
k_n(GPa/m)	k_s(GPa/m)	f_T(MPa)	c(MPa)	ϕ(°)
45	18	0.2	0.3	35
Contact properties between the soil and masonry				
k_n(GPa/m)	k_s(GPa/m)	f_T(MPa)	c(MPa)	ϕ(°)
45	18	0	0	20

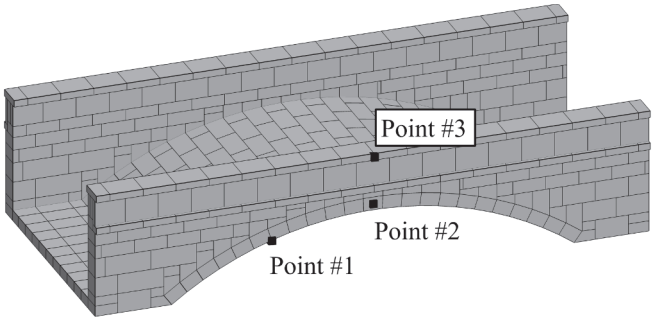

Fig. 12. The points where the displacements are measured.

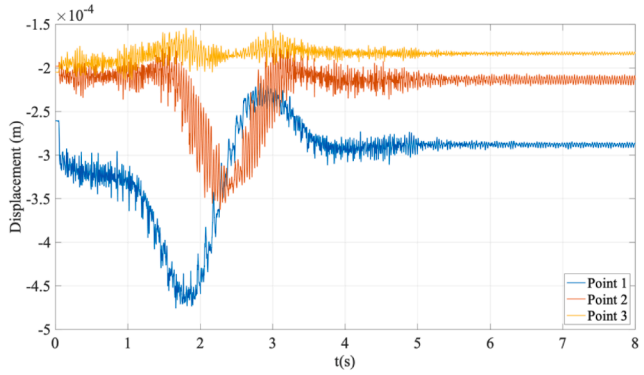

Fig. 13. Displacement time history of three points on the arch under moving load analysis.

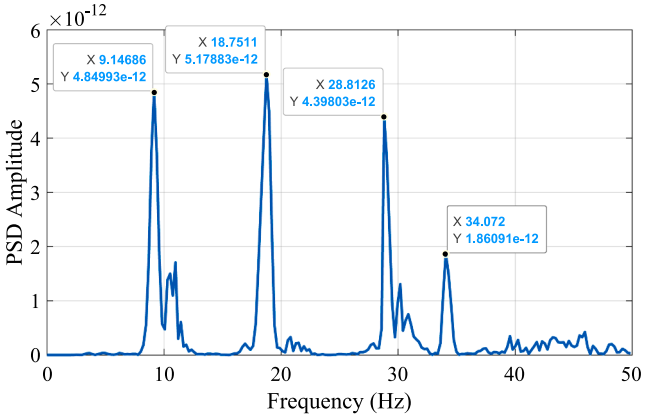

Fig. 14. Power Spectrum of the displacement time-history at the quarter span.

ii. Extract the modal damping ratios for each mode for the un-damped model and compare them with the experimental values presented in this study or recommended values in the literature.
iii. If the damping inherent in the MDC model is not sufficient, supplementary damping in the form of mass-proportional damping or Rayleigh damping can be added. As discussed before, the modal damping ratios extracted from experiments can be best simulated by Rayleigh damping anchored at the first and n^{th} modal frequencies n being the highest mode included in the analysis. However, in DEM, as mentioned previously, stiffness-proportional component of the Rayleigh damping leads often to very small time-steps and, thus, high computational costs. Mass-proportional damping provides an excellent alternative because, as shown in this study, it emulates the experimental behavior in a satisfactory manner and does not impact the computational cost of the numerical analysis.

6. Concluding remarks

In this article, we present the damping behavior of masonry arch bridges under service loads extracted from experiments and provide guidelines on how to emulate this behavior in numerical analysis, particularly in mixed discrete-continuum model applications. First, an experimental campaign where the vibrations on three masonry arch bridges were monitored under a train load is presented. The modal damping ratios from different sensors on each of the bridges were extracted by isolating the modal component of the vibrations during free decay after the train leaves the bridge. A single-arch masonry bridge was modeled using mixed discrete continuum approach and a moving load analysis was conducted without applying any additional viscous damping to evaluate the inherent damping in MDC models provided by their nonlinear nature. As a result of these evaluations, the following conclusions can be drawn:

- For a given bridge, there is variation in the modal damping ratios extracted from different sensors and train crossings. This variation increases from one bridge to another, but, despite this variation, some general trends can be clearly observed.
- Experimental data shows that the modal damping ratios in masonry arch bridges are highest for the first mode and decreases for the higher modes. Therefore, stiffness-proportional damping, where the

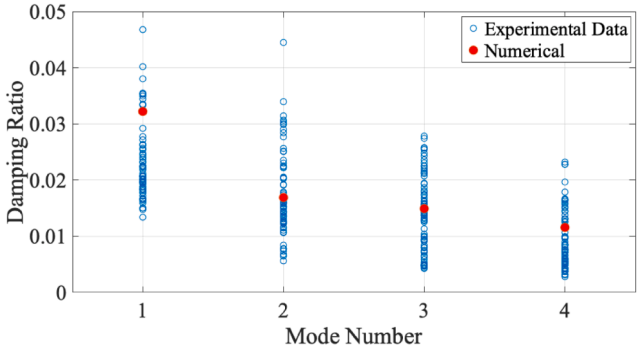

Fig. 16. Experimental and modal damping ratios.

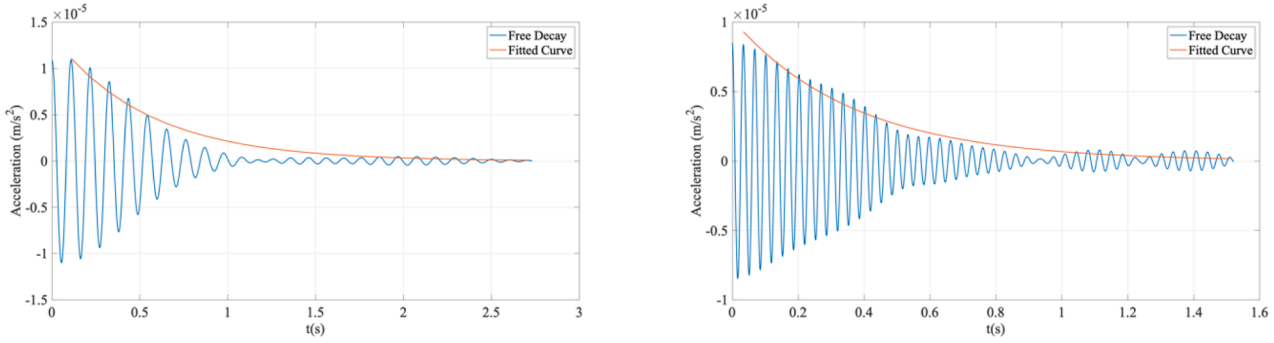

(a) First mode component (f = 9.14 Hz) (b) Third mode component (f = 28.81 Hz)

Fig. 15. First and third mode components of the free decay of the vibrations at the quarter span of the bridge and the fitted exponential curves to estimate the modal damping ratios.

modal damping ratios increase with the modal frequency, is not suitable to model the damping behavior of masonry arch bridges under service loads.

- The damping in the monitored bridges under service loads were observed to be much higher than the damping under the ambient vibrations. Because damping is related to several mechanisms such as sliding and opening and closing of the cracks, the amplitude of the loading and the resulting vibrations play a significant role in the amount of damping. Therefore, the damping values extracted from ambient vibrations are likely to underestimate the damping in masonry arch bridges under service loads.
- Rayleigh damping anchored at the 1st and n^{th} modal frequencies, n being the highest mode number that will be considered in the analysis, provides the best alternative to emulate the damping behavior of masonry arch bridges. We recommend using this damping model in finite element or discrete element applications, both in macro- and micro-modeling, where the damping model has no impact on the computational costs.
- For discrete element models, the stiffness-proportional component of the Rayleigh damping can adversely impact the computational cost. For such models, mass-proportional damping provides a very attractive alternative because it can emulate the damping behavior of masonry arch bridges under service loads satisfactorily and has no impact on the computational costs.
- In literature, several studies refrain from using mass-proportional damping in seismic analysis using discrete element models because the reduction in modal frequencies due to damage under seismic loads can lead to very high modal damping ratios for the first mode. However, such a concern is not relevant for analysis of masonry arch bridges under service loads because the frequency of the structure should not vary under these loads as no sudden damage is expected.
- Moving load analysis on a single-span masonry arch bridge modeled using MDC approach without providing any additional viscous damping showed that the inherent damping in MDC models provided by the nonlinear behavior at the joints and the soil continuum can be sufficient to emulate the damping behavior in masonry arch bridges. Therefore, the analysts are urged to first conduct an analysis without additional damping and evaluate the inherent energy dissipation in MDC models. In case the damping inherent in the model is deemed to be insufficient, additional damping can be provided as Rayleigh damping or mass-proportional damping.

Experimental research that studies the damping of masonry arch bridges under service loads is scarce. This study shows that damping extracted from ambient vibrations is likely to be lower compared to the damping under service loads. More research that focuses on damping of masonry arch bridges under service loads is necessary to be able to understand and emulate the behavior of these structures under such loads.

CRediT authorship contribution statement

Emrah Erduran: Conceptualization, Methodology, Formal analysis, Visualization, Writing – original draft. **Semih Gonen:** Investigation, Conceptualization, Visualization, Writing – original draft. **Bora Pulatsu:** Formal analysis, Visualization, Conceptualization, Writing – original draft. **Serdar Soyoz:** Resources, Funding acquisition, Writing – review & editing.

Declaration of Competing Interest

The authors declare that they have no known competing financial interests or personal relationships that could have appeared to influence the work reported in this paper.

Data availability

Data will be made available on request.

References

[1] Bell B. D1.2 European Railway Bridge Demography. Sustainable Bridges – Assessment for Future Traffic Demands and Longer Lives. 2004.
[2] Helmerich R, Niederleithinger E, Trela C, Bień J, Kamiński T, Bernardini G. Multi-tool inspection and numerical analysis of an old masonry arch bridge. Struct Infrastruct Eng 2012;8:27–39. https://doi.org/10.1080/15732471003645666.
[3] Sarhosis V, De Santis S, de Felice G. A review of experimental investigations and assessment methods for masonry arch bridges. Struct Infrastruct Eng 2016;12:1439–64. https://doi.org/10.1080/15732479.2015.1136655.
[4] Tapkın S, Tercan E, Siphesihle Motsa M, Drosopoulos G, Stavroulaki M, Maravelakis E, et al. Structural investigation of masonry arch bridges using various nonlinear finite-element models. J Bridg Eng 2022;27:04022053. https://doi.org/10.1061/(ASCE)BE.1943-5592.0001870.
[5] Oliveira DV, Lourenço PB, Lemos C. Geometric issues and ultimate load capacity of masonry arch bridges from the northwest Iberian Peninsula. Eng Struct 2010;32:3955–65. https://doi.org/10.1016/J.ENGSTRUCT.2010.09.006.
[6] Milani G, Lourenço PB. 3D non-linear behavior of masonry arch bridges. Comput Struct 2012;110–111:133–50. https://doi.org/10.1016/J.COMPSTRUC.2012.07.008.
[7] Pulatsu B, Erdogmus E, Lourenço PB. Comparison of in-plane and out-of-plane failure modes of masonry arch bridges using discontinuum analysis. Eng Struct 2019;178:24–36. https://doi.org/10.1016/J.ENGSTRUCT.2018.10.016.
[8] Fanning PJ, Boothby TE. Three-dimensional modelling and full-scale testing of stone arch bridges. Comput Struct 2001;79:2645–62. https://doi.org/10.1016/S0045-7949(01)00109-2.
[9] Carr AJ, Jáuregui DV, Riveiro B, Arias P, Armesto J. Structural evaluation of historic masonry arch bridges based on first hinge formation. Constr Build Mater 2013;47:569–78. https://doi.org/10.1016/J.CONBUILDMAT.2013.05.084.
[10] Costa C, Arêde A, Morais M, Aníbal A. Detailed FE and DE modelling of stone masonry arch bridges for the assessment of load-carrying capacity. Procedia Eng 2015;114:854–61. https://doi.org/10.1016/J.PROENG.2015.08.039.
[11] Tubaldi E, Minga E, Macorini L, Izzuddin BA. Mesoscale analysis of multi-span masonry arch bridges. Eng Struct 2020;225:111137. https://doi.org/10.1016/j.engstruct.2020.111137.
[12] Sayin E. Nonlinear seismic response of a masonry arch bridge. Earthq Struct 2016;10(2):483–94.
[13] Karaton M, Aksoy HS, Sayın E, Calayır Y. Nonlinear seismic performance of a 12th century historical masonry bridge under different earthquake levels. Eng Fail Anal 2017;79:408–21. https://doi.org/10.1016/j.engfailanal.2017.05.017.
[14] Gonen S, Pulatsu B, Erdogmus E, Karaesmen E, Karaesmen E. Quasi-static nonlinear seismic assessment of a Fourth Century A.D. Roman Aqueduct in Istanbul, Turkey. Heritage 2021;4:401–21. https://doi.org/10.3390/heritage4010025.
[15] Gönen S, Soyöz S. Reliability-based seismic performance of masonry arch bridges. Struct Infrastruct Eng 2021:1–16. https://doi.org/10.1080/15732479.2021.1918726.
[16] Demirel IO, Aldemir A. Simplified approach for seismic performance assessment of dry-joint masonry arch bridges. Buildings 2021;11(7):313. https://doi.org/10.3390/buildings11070313.
[17] Gözde Çubuk E, Sayin E, Özmen A, Mühendisliği İ, Üniversitesi F, Fakültesi M, et al. Dynamic analysis of historical masonry arch bridges under different earthquakes: the case of Murat Bey Bridge. Turkish J Sci Technol 2022;17:461–73.
[18] Pelà L, Aprile A, Benedetti A. Comparison of seismic assessment procedures for masonry arch bridges. Constr Build Mater 2013;38:381–94. https://doi.org/10.1016/J.CONBUILDMAT.2012.08.046.
[19] Zampieri P, Zanini MA, Faleschini F, Hofer L, Pellegrino C. Failure analysis of masonry arch bridges subject to local pier scour. Eng Fail Anal 2017;79:371–84. https://doi.org/10.1016/J.ENGFAILANAL.2017.05.028.
[20] Scozzese F, Ragni L, Tubaldi E, Gara F. Modal properties variation and collapse assessment of masonry arch bridges under scour action. Eng Struct 2019;199:109665. https://doi.org/10.1016/j.engstruct.2019.109665.
[21] De Felice G, De Santis S. Experimental and numerical response of arch bridge historic masonry under eccentric loading. Int J Archit Herit 2010;4:115–37. https://doi.org/10.1080/15583050903093886.
[22] Orbán Z, Gutermann M. Assessment of masonry arch railway bridges using non-destructive in-situ testing methods. Eng Struct 2009;31:2287–98. https://doi.org/10.1016/J.ENGSTRUCT.2009.04.008.
[23] Pellegrino C, Zanini MA, Zampieri P, Modena C. Contribution of in situ and laboratory investigations for assessing seismic vulnerability of existing bridges. Struct Infrastruct Eng 2015;11:1147–62. https://doi.org/10.1080/15732479.2014.938661.
[24] Acikgoz S, DeJong MJ, Kechavarzi C, Soga K. Dynamic response of a damaged masonry rail viaduct: Measurement and interpretation. Eng Struct 2018;168:544–58. https://doi.org/10.1016/J.ENGSTRUCT.2018.04.054.
[25] Domede N, Sellier A, Stablon T. Structural analysis of a multi-span railway masonry bridge combining in situ observations, laboratory tests and damage modelling. Eng Struct 2013;56:837–49. https://doi.org/10.1016/J.ENGSTRUCT.2013.05.052.

[26] Solla M, Riveiro B, Lorenzo H, Armesto J. Ancient stone bridge surveying by ground-penetrating radar and numerical modeling methods. J Bridg Eng 2014;19:110–9. https://doi.org/10.1061/(ASCE)BE.1943-5592.0000497.
[27] Banerji P, Chikermane S. Condition assessment of a heritage arch bridge using a novel model updation technique. J Civ Struct Heal Monit 2012;2:1–16. https://doi.org/10.1007/s13349-011-0013-9.
[28] Srinivas V, Sasmal S, Ramanjaneyulu K, Ravisankar K. Performance evaluation of a stone masonry-arch railway bridge under increased axle loads. J Perform Constr Facil 2014;28:363–75. https://doi.org/10.1061/(asce)cf.1943-5509.0000407.
[29] Brencich A, Sabia D. Experimental identification of a multi-span masonry bridge: The Tanaro Bridge. Constr Build Mater 2008;22:2087–99. https://doi.org/10.1016/J.CONBUILDMAT.2007.07.031.
[30] Gonen S, Soyoz S. Dynamic identification of masonry arch bridges using multiple methodologies. Conf. Proc. Soc. Exp. Mech. Ser., Springer; 2021, p. 37–47. 10.1007/978-3-030-47709-7_4.
[31] Costa C, Arêde A, Costa A, Caetano E, Cunha Á, Magalhães F. Updating numerical models of masonry arch bridges by operational modal analysis. Int J Archit Herit 2015;9:760–74. https://doi.org/10.1080/15583058.2013.850557.
[32] Aoki T, Sabia D, Rivella D, Komiyama T. Structural characterization of a stone arch bridge by experimental tests and numerical model updating. Int J Archit Herit 2007;1:227–50. https://doi.org/10.1080/15583050701241208.
[33] Aytulun E, Soyoz S, Karcioglu E. System identification and seismic performance assessment of a stone arch bridge. J Earthq Eng 2022;26(2):723–43.
[34] Civera M, Calamai G, Zanotti FL. System identification via Fast Relaxed Vector Fitting for the Structural Health Monitoring of masonry bridges. Structures 2021;30:277–93. https://doi.org/10.1016/j.istruc.2020.12.073.
[35] Civera M, Mugnaini V, Zanotti FL. Machine learning-based automatic operational modal analysis: a structural health monitoring application to masonry arch bridges. Struct Control Heal Monit 2022;29:1–23. https://doi.org/10.1002/stc.3028.
[36] Costa C, Ribeiro D, Jorge P, Silva R, Arêde A, Calçada R. Calibration of the numerical model of a stone masonry railway bridge based on experimentally identified modal parameters. Eng Struct 2016;123:354–71. https://doi.org/10.1016/J.ENGSTRUCT.2016.05.044.
[37] Borlenghi P, Saisi A, Gentile C. ND testing and establishing models of a multi-span masonry arch bridge. J Civ Struct Heal Monit 2023. https://doi.org/10.1007/s13349-022-00666-1.
[38] Bautista-De Castro Á, Sánchez-Aparicio LJ, Carrasco-García P, Ramos LF, González-Aguilera D. A multidisciplinary approach to calibrating advanced numerical simulations of masonry arch bridges. Mech Syst Sig Process 2019;129:337–65. https://doi.org/10.1016/j.ymssp.2019.04.043.
[39] Lorenzoni F, De Conto N, da Porto F, Modena C. Ambient and free-vibration tests to improve the quantification and estimation of modal parameters in existing bridges. J Civ Struct Heal Monit 2019;9:617–37. https://doi.org/10.1007/s13349-019-00357-4.
[40] Reccia E, Milani G, Cecchi A, Tralli A. Full 3D homogenization approach to investigate the behavior of masonry arch bridges: the Venice trans-lagoon railway bridge. Constr Build Mater 2014;66:567–86. https://doi.org/10.1016/j.conbuildmat.2014.05.096.
[41] Azimi P, Yazdani M. Calculation of dynamic amplification factor for railway concrete and masonry arch bridges subjected to high-speed trains. Period Polytech Civ Eng 2022;66:876–90. https://doi.org/10.3311/PPci.19494.
[42] Bozyigit B, Acikgoz S. Dynamic amplification in masonry arch railway bridges. Structures 2022;45:1717–28. https://doi.org/10.1016/j.istruc.2022.09.100.
[43] Forgács T, Sarhosis V, Ádány S. Shakedown and dynamic behaviour of masonry arch railway bridges. Eng Struct 2021;228:111474. https://doi.org/10.1016/j.engstruct.2020.111474.
[44] Yazdani M, Azimi P. Assessment of railway plain concrete arch bridges subjected to high-speed trains. Structures 2020;27:174–93. https://doi.org/10.1016/j.istruc.2020.05.042.
[45] Sarhosis V, Forgács T, Lemos JV. A discrete approach for modelling backfill material in masonry arch bridges. Comput Struct 2019;224:106108. https://doi.org/10.1016/j.compstruc.2019.106108.
[46] Kishen JMC, Ramaswamy A, Manohar CS. Safety assessment of a masonry arch bridge: field testing and simulations. J Bridg Eng 2013;18:162–71. https://doi.org/10.1061/(asce)be.1943-5592.0000338.
[47] Lemos JV, Sarhosis V. Dynamic analysis of masonry arches using Maxwell damping. Structures 2023;49:583–92. https://doi.org/10.1016/j.istruc.2023.01.139.
[48] Galvez F, Sorrentino L, Dizhur D, Ingham JM. Damping considerations for rocking block dynamics using the discrete element method. Earthq Eng Struct Dyn 2022;51(4):935–57.
[49] Dimitri R, De Lorenzis L, Zavarise G. Numerical study on the dynamic behavior of masonry columns and arches on buttresses with the discrete element method. Eng Struct 2011;33:3172–88. https://doi.org/10.1016/j.engstruct.2011.08.018.
[50] Pulatsu B, Kim S, Erdogmus E, Lourenço PB. Advanced analysis of masonry retaining walls using mixed discrete-continuum approach. Proc Inst Civ Eng - Geotech Eng 2020:1–34. https://doi.org/10.1680/jgeen.19.00225.
[51] Savalle N, Vincens E, Hans S, Lourenço PB. Dynamic numerical simulations of dry-stone retaining walls: identification of the seismic behaviour factor. Geosciences 2022;12:252. https://doi.org/10.3390/geosciences12060252.
[52] Quezada JC, Vincens E, Mouterde R, Morel JC. 3D failure of a scale-down dry stone retaining wall: a DEM modelling. Eng Struct 2016;117:506–17. https://doi.org/10.1016/j.engstruct.2016.03.020.
[53] Bettinelli L, Glatz B, Stollwitzer A, Fink J. Comparison of different approaches for considering vehicle-bridge-interaction in dynamic calculations of high-speed railway bridges. Eng Struct 2022;270:114897. https://doi.org/10.1016/j.engstruct.2022.114897.
[54] Gönen S, Soyöz S. Seismic analysis of a masonry arch bridge using multiple methodologies. Eng Struct 2021;226:111354. https://doi.org/10.1016/j.engstruct.2020.111354.
[55] Brincker R, Zhang L, Andersen P. Modal identification of output-only systems using frequency domain decomposition. Smart Mater Struct 2001;10:441–5. https://doi.org/10.1088/0964-1726/10/3/303.
[56] Chopra AK. Dynamics of Structures: Theory and Applications to Earthquake Engineering. 5th Editio. Pearson; 2017.
[57] Cundall PA. Formulation of a three-dimensional disctinct element model - Part I. A scheme to detect and represent contacts in a system composed of many polyhedral blocks. Int J Rock Mech Min Sci Geomech 1988;25:107–16.
[58] Lemos JV. Contact representation in rigid block models of masonry. Int J Mason Res Innov 2017;2:321. https://doi.org/10.1504/ijmri.2017.10008298.
[59] Itasca Consulting Group Inc. 3DEC Three Dimensional Distinct Element Code 2013.
[60] Erdogmus E, Pulatsu B, Gaggioli A, Hoff M. Reverse engineering a fully collapsed ancient roman temple through geoarchaeology and DEM. Int J Archit Herit 2021;15(12):1795–815.
[61] Çaktı E, Saygılı Ö, Lemos JV, Oliveira CS. Discrete element modeling of a scaled masonry structure and its validation. Eng Struct 2016;126:224–36. https://doi.org/10.1016/J.ENGSTRUCT.2016.07.044.